A numerical prediction of fiber orientation in hydrogels for extrusion-based 3D printing

van Than Mai, Romain Rieger, Robin Chatelin, Edwin-Joffrey Courtial, Caroline Boulocher

A numerical prediction of fiber orientation in hydrogels for extrusion-based 3D printing

V.T. MAI [a,b], R. RIEGER[a,b], R. CHATELIN[c], E.-J. COURTIAL[d], C. BOULOCHER[e]

a. Univ. Lyon, VetAgro Sup, UPSP ICE 2021.A, France, van.mai@vetagro-sup.fr
b. Univ. Lyon, École Centrale de Lyon, France, romain.rieger@ec-lyon.fr
c. Univ. Lyon, École Centrale de Lyon–ENISE, LTDS UMR CNRS 5513, France, robin.chatelin@enise.fr
d. Univ. Lyon, UCBL, ICBMS UMR CNRS 5246, France, edwin.courtial@univ-lyon1.fr
e. UniLaSalle Polytechnic Institute, Veterinary College, Campus of Rouen, France, caroline.boulocher@unilasalle.fr

Abstract

The purpose of this study is to develop a numerical strategy able to compute and predict the flow-induced orientation of the fibers within an hydrogel during extrusion-based 3D printing process. The probability distribution function approach was used to describe the orientation of a fiber population. This approach was coupled to a computational fluid dynamic (CFD) method to compute the fluid flow which transports the fibers. Numerical computations were performed for a planar channel and a conical nozzle geometry. The results showed that the fiber orientation during the extrusion process is delayed by the hydrogel rheological behavior while the final fiber orientation remains the same. This study presents the first analysis for the fiber orientation prediction in hydrogel for extrusion-base 3D printing.

Keywords: 3D printing, Extrusion, Fiber orientation, Rheology, Probability distribution function.

1 Introduction

Extrusion-based 3D printing is an additive manufacturing technique to produce cellularized scaffolds for personalized tissue-engineering applications [1]. The extrusion process has a strong impact on the final mechanical behavior as well on the oriented engineered tissue [2]. Cellularized scaffolds are usually made from hydrogel [3,4] which can be reinforced by rigid fibers such as cellulose or carbon nanofibers [2, 5–8]. Therefore, the overall aim of this work is to develop a numerical model able to compute and predict the flow-induced orientation of rigid fibers within an hydrogel. As a first step, an acellularized hydrogel was investigated.

At a given space position, several approaches have been used to represent the fiber orientation state [9]. One possible representation of the fiber orientation state is to use the second order orientation tensor introduced by Advani and Tucker [10]. The equation describing the rate of change of this tensor involves

a fourth order orientation tensor. When derived, a sixth order orientation tensor appears which leads to an infinite serie of evolution equations [9] and therefore requires a supplement linear or quadratic equation called a closure approximation to close the problem. This raises the problem of choosing an accurate closure approximation to prevent the loss of physical properties in the orientation tensor describing the physical state of the fibers. Another possibility is to use the probability distribution function (PDF), which is the most general description of fiber orientation state. PDF is defined, such that $\psi(\overrightarrow{x}, \overrightarrow{p}, t)$ represents the probability to find at the position $\overrightarrow{x}$ a fiber at an orientation $\overrightarrow{p}$ at a given time t. The continuity condition describes the change of rate of ψ with respect to time when fiber orientation is changing:

$$\frac{D\psi}{Dt} = -\frac{\partial}{\partial \overrightarrow{p}}.(\psi \dot{\overrightarrow{p}}) \tag{1}$$

Where D/Dt represents the material derivative, $\dot{\overrightarrow{p}}$ is the motion of a fiber. The direct calculation enabled by the use of the PDF approach was chosen to predict the fiber orientation in this work. The fibers were assumed as rigid cylinders and considered distributed spatially homogeneous in the computed domain. Furthermore, we focused on a 2D problem reducing to two spatial variables (x, y) related to the spatial position of the center of the fiber, and to one angle variable (θ) related to the fiber orientation distribution. The paper is organized as follows: firstly, a mathematical modeling was used to solve the equation 1 for ψ, later called the Fokker-Planck equation, in a fluid flow problem using the Navier-Stokes equations. Then, fiber orientation was analysed with respect to the rheological behavior of the fluid (representing the hydrogel) and two different geometries were compared. Finally, conclusions and perspectives are discussed.

2 Mathematical modeling

2.1 Fiber orientation distribution model

A single and rigid fiber is usually given by the unit vector $\overrightarrow{p}$ directed along its principal axis (see Figure1(A)). In the 2D case the orientation of each fiber can be expressed as:

$$\overrightarrow{p} = \begin{pmatrix} \sin\theta \\ \cos\theta \end{pmatrix}$$

Jeffery [11] developed the first description of the motion of a single fiber as shown in the first two terms of the right hand-side of equation (2):

$$\dot{\overrightarrow{p}} = \mathbf{W}.\overrightarrow{p} + \lambda[\mathbf{D}.\overrightarrow{p} - \mathbf{D} : (\overrightarrow{p} \otimes \overrightarrow{p})\overrightarrow{p}] - \frac{D_r}{\psi}\frac{\partial \psi}{\partial \overrightarrow{p}} \tag{2}$$

where $\overrightarrow{u}$ is the fluid velocity, $\mathbf{W} = \frac{1}{2}\left[(\nabla \overrightarrow{u}) - (\nabla \overrightarrow{u})^T\right]$ is the vorticity tensor, $\mathbf{D} = \frac{1}{2}\left[(\nabla \overrightarrow{u}) + (\nabla \overrightarrow{u})^T\right]$ is the deformation rate tensor. The particle shape function $\lambda = (r_e^2 - 1)/r_e^2 + 1)$ related to the aspect ratio of the fiber $r_e = L/D$ where L and D being its length and diameter, respectively. The last term in the right-hand side of equation (2) was introduced by Folgar and Tucker [12] to take into account fiber interaction to predict the orientation in semi-dilute and concentrated solutions where $D_r = C_I\dot{\gamma}$, $\dot{\gamma} = \sqrt{2\mathbf{D} : \mathbf{D}}$ denotes the scalar magnitude of the rate of the strain tensor and C_I describes the interaction coefficient. Combining the continuity equation (1) for the PDF with the equation (2) it produces

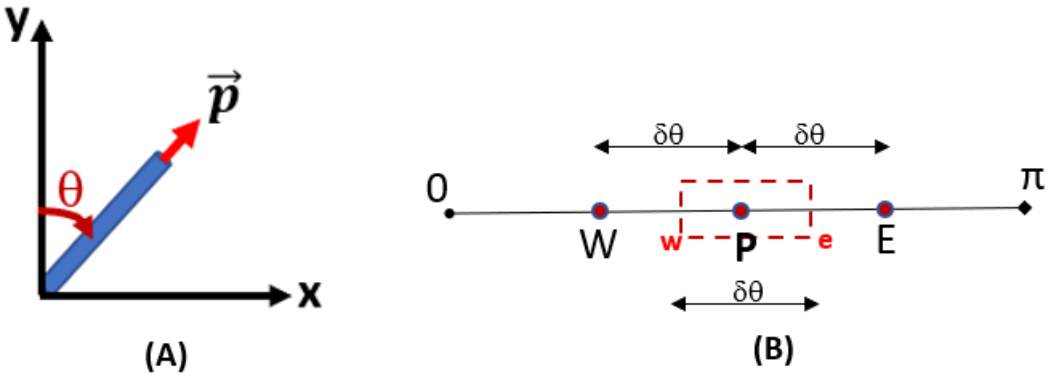

Figure 1: (A) Schematic of a unit vector $\overrightarrow{p}$, (B) Schematic of the discretized control volume in the FVM. P, E and W represent the nodal point , the faces in east and west, respectively.

the rate of change with time for ψ as:

$$\frac{D\psi}{Dt} = -\frac{\partial}{\partial \overrightarrow{p}}.(\psi \dot{\overrightarrow{p}}) + D_r \bigtriangledown_p^2 \psi \tag{3}$$

Where $D/Dt = \partial\psi/\partial t + \overrightarrow{u}.\nabla_x\psi$, $\overrightarrow{u}$ is the fluid velocity obtained from the Navier-Stokes equations, $\bigtriangledown_p^2$ refers to $\partial^2/\partial\overrightarrow{p}^2$. Equation (3) is known as the Fokker-Planck (FP) equation and needs to be solved to find the orientation of a fiber population at a given spatial position. However, equation 3 is multi-dimensional due to the dependence of $\psi(\overrightarrow{x}, \overrightarrow{p}, t)$ on the spatial and angle variable $\overrightarrow{p}(\theta)$. Therefore, in this work a numerical strategy was proposed to deal with this problem using Comsol-Multiphysics (v5.6) with two discretization steps [13] [14] : (i) First, a discretization of the FP equation based on Finite Volume Method (FVM) in the angle domain $\overrightarrow{p}(\theta)$. Figure 1(B) illustrates the basic control volume on which we carried out the discretization of the FP equation. At this stage, a system of equation at a general point P and its neighbors W and E was formed as following:

$$\delta\theta.\overrightarrow{u}.\nabla_x\psi_P + a_P\psi_P - a_W\psi_W - a_E\psi_E = 0 \tag{4}$$

The expressions for coefficients a_P, a_W, a_E at each node of the FVM mesh are detailed in the work of Mezi *et al.,* [14]. (ii) Then, the FP equation (equation (4)) obtained from the previous step is discretized and implemented into the partial differential equation (PDE) interface in Comsol-Multiphysics. The PDE equation type used is identical to the convection-diffusion problem. This strategy enables the resolution of an equations system discretized with FVM coupled to the finite element resolution of a fluid problem in the spatial domain. In this work a 2D stationary resolution is assumed as a first approach in order to reduce variables in both spatial and angle domains. Moreover, we did not considered any interaction between the fibers leading to fix the dimensionless parameter $C_I = 10^{-2}$ [14]. Finally, the fibers are considered as rigid cylinders, thus thickness can be ignored leading to $\lambda = 1$.

2.2 Flow field equations

The hydrogel was modeled using two type of rheological behaviors for the fluid flow. As a first approximation and to test of the flow-induced fiber orientation, we assume a Newtonian and incompressible fluid [15], with a viscosity $\mu = 0.1Pa.s$ and a density $\rho = 850kg/m^3$.

Then, we considered a non-Newtonian fluid consisting of three main components: Fibrinogen, Alginate and Gelatin (FAG) described by Pourchet *et al.,* [16]. The rheological characterization of the FAG was

performed on a rotational rheometer (DHR2, TA instruments, USA) with the protocol described in [17]. The results (not presented in this article) shows that a Herschel-Bulkley model is suitable:

$$\tau = \tau_0 + k\dot{\gamma}^n \tag{5}$$

where τ is the shear stress [Pa], τ_0 the static yield stress [Pa], k the consistency index [Pa.s], $\dot{\gamma}$ the shear rate [s] and n the flow index [-]. If $\tau < \tau_0$ the Herschel-Bulkley fluid behaves as a rigid (non-deformable) solid, otherwise it behaves as a fluid. Rheological parameters were determined by a numerical least square minimization using a Levenberg-Marquardt nonlinear regression algorithm giving: $\tau_0 = 113.96$ [Pa], $k = 195.36$ [Pa.s] and $n = 0.43$.

In order to characterize the flow regime, the Reynolds number (Re) was determined which correlates the inertia forces to the viscous forces and can be defined as:

$$Re = \frac{\rho V l}{\mu} \tag{6}$$

where ρ is the density of the fluid $[kg/m^3]$, V the average velocity $[m/s]$, l the characteristic length $[m]$ and μ the dynamic viscosity of the fluid $[Pa.s]$. The results obtained from calculating the Reynolds number for both fluids flow (Newtonian and Herschel-Bulkley) are low, typically in the range of [0.0051 - 102] showing that the flows are considered to be laminar (also known as viscous flow).
The Bingham number (Bm), a dimensionless number used in rheology to characterize the relationship between the yield stress and the viscous stress was calculated for the Herschel-Bulkley fluid case:

$$Bm = \frac{\tau_0 l}{\mu V} \tag{7}$$

where τ_0 is the static yield stress $[Pa]$, l the characteristic length $[m]$, V the average velocity $[m/s]$, and μ the dynamic viscosity of the fluid $[Pa.s]$. The results of Bm are very small, in the range of [0.00077-0.62].
The equation (4) is a typical convection-diffusion system where the convection dominates the fluid flow regime leading to numerical instabilities. An artificial diffusion coefficient D_{num} can be added to stabilize the numerical convergence. In this case, the Péclet number (Pe) enables the estimation of convection versus diffusion regime was calculated as:

$$Pe = \frac{V l}{D_{num}} \tag{8}$$

where V is the average velocity $[m/s]$, l the characteristic length $[m]$ and D_{num} the artificial diffusion coefficient $[m^2/s]$. In this study, we did not consider any effect of the D_{num} on the numerical model, setting D_{num} = 10E-5 [14], therefore Pe = [9.6-120].

2.3 Geometrical models and boundary conditions

Two geometries are presented in this study. An axisymmetric planar channel and a 2D conical nozzle as depicted in Figure 2 with their respective boundary conditions (BC). The planar channel is a rectangle of 4x2 mm^2. The conical nozzle has a length of 30 mm and an inner diameter of 200 µm (Optimum®, Nordson EFD, USA). Regarding the planar channel the symmetry around the x-direction, only half of the rectangle was considered using axisymmetric modeling to reduce the computation time. At the exit of the planar channel (BC3) and the conical nozzle (BC3') a normal flow was imposed to suppress back flow.

The constant flow rate of $5\mu l/s$ (BC3) was defined to be compatible with bioprinting conditions [18]. The domain was discretized with 3323 triangles elements for the planar channel and 7777 triangles elements for conical nozzle. Finally, all fibers were assumed to be isotropic at the inlet (BC1 and BC1') leading to impose at a boundary condition of $\psi = 1/\pi$ in the Fokker-Planck equation [14].

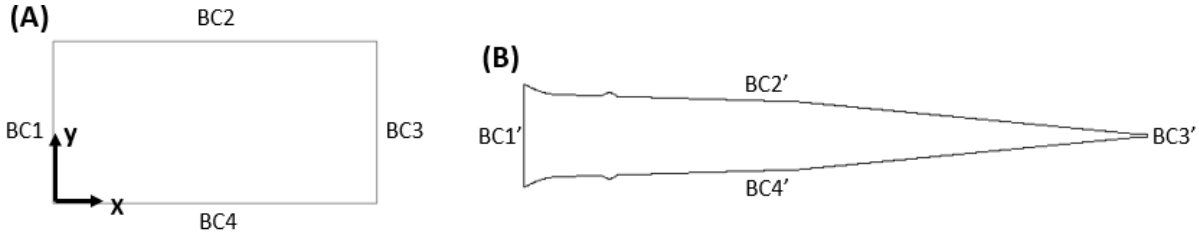

Figure 2: Boundary conditions : (A) Axisymmetric planar channel geometry - BC1: $P_{in} = 600$ Pa, $\psi = 1/\pi$; BC2: zero-slip; BC3: $P_{out} = 0$ Pa; BC4: symmetric condition. (B) 2D Conical nozzle geometry - BC1': $V_{in} = 5\ \mu l/s$, $\psi = 1/\pi$; BC2': zero-slip; BC3': $P_{out} = 0$ Pa; BC4': zero-slip. Non dimensional numbers : (A) Re = [0.06-102], Bm = 0.00077, Pe = 120. (B) Re = [0.0051-8.16], Bm = 0.62, Pe = 9.6.

3 Results and discussion

3.1 Planar channel axisymmetric poiseuille flow

Firstly, a case study consisting of 2D extrusion in a planar channel for Newtonian and Herschel-Bulkley behaviors was considered. The flow was a poiseuille type, one of the most basic flow we choose to investigate the fiber orientation [14]. The effective deformation distribution over the calculated domain is depicted in Figure 3 for these two behaviors. The white ellipses (Newtonian case) and the magenta ellipses (Herschel-Bulkley case) were formed from the eigenvalues and eigenvectors directly calculated from the PDF results as: $\langle \overrightarrow{p}\,\overrightarrow{p} \rangle = \int_p p_i p_j \psi dp,\ i,j = 1,n$ to represent the average fiber orientation, where $n = 30$ represents the discretization in the FVM. For both rheological behaviors, the ellipses initially circular, becomes gradually elongated along their major axes showing fibers alignment in the direction of the flow. Furthermore, near the wall where the shear rate is the highest, the ellipses are flattened which means that the fibers are more quickly oriented.

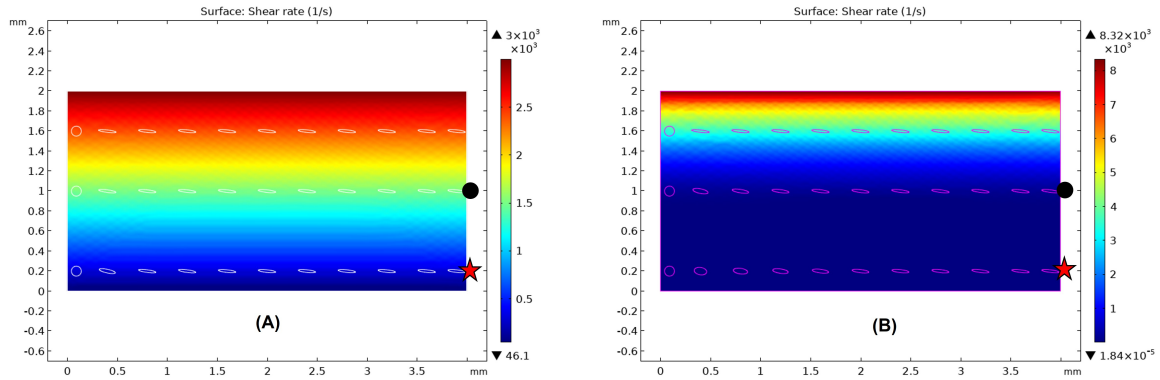

Figure 3: Shear rate distribution of fluid domain. (A) Newtonian; (B) Herschel-Bulkley. The white ellipses represent the average fiber orientation.

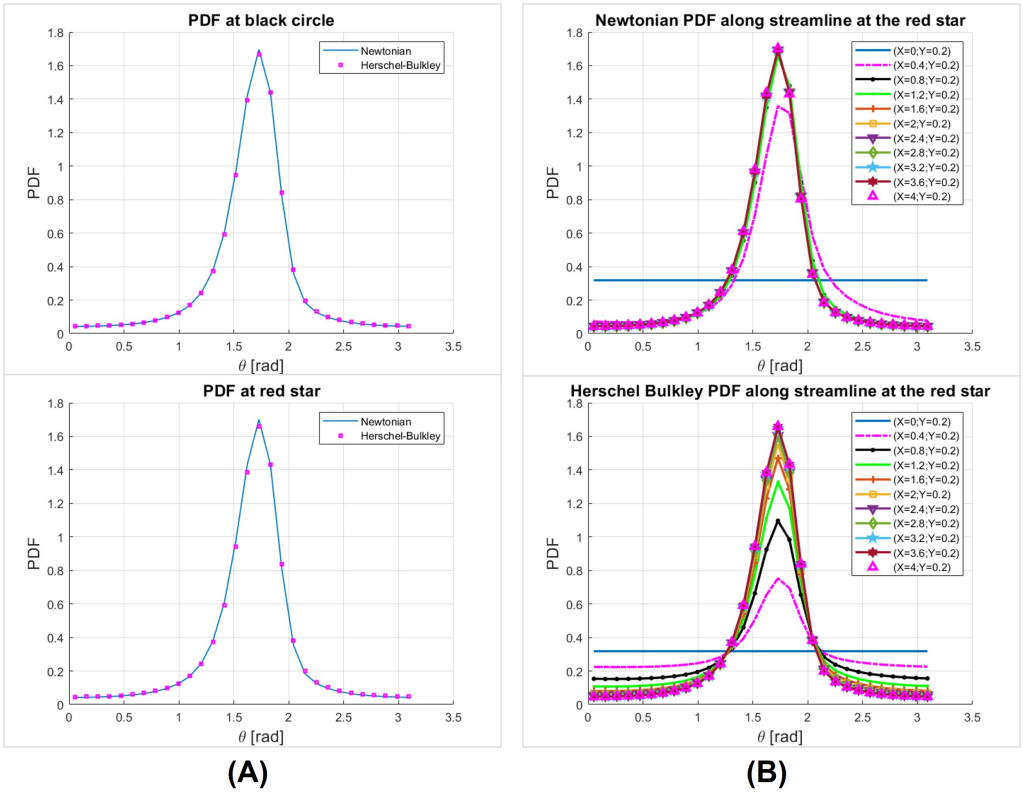

Figure 4: PDF curves compared for Newtonian and Herschel-Bulkley. (A) Comparison of PDF at two points (black circle and red star represented in Figure 3); (B) PDF along an horizontal streamline passing at the "red star" point ($y = 0.2$ mm).

In Figure 4(A) the PDF at the outlet of the channel for two points (black circle [x=4;y=1] and red star [x=4;y=0.2]) are depicted. The exact same distributions are observed for Newtonian and Herschel-Bulkley behavior.

The case study on an axisymmetric planar channel with poiseuille flow shows that the fluid rheological behavior does not affect the fiber orientation at the outlet of the channel. Most of the fibers have an orientation angle of $\pi/2$ meaning that they are aligned with the direction of the flow. However, the results in Figure 4(B) show that the rheological behavior affects the characteristic geometrical length along the streamline at which the orientation's steady state is reached. Indeed for a Newtonian behavior the fibers align along the streamline in a very little characteristic length (at $x = 1.2$ mm) compared to Herschel-Bulkley (at $x = 3.6$ mm).

3.2 Ink flow through conical nozzle

Secondly, we reproduced a bioprinting process using the same extrusion conditions as Lemarié *et al.,* [17] in order to predict fiber orientation induced by the flow through a conical nozzle. An Herschel-Bulkley rheological behavior was chosen for this case because its rheological properties provide a dual capacity, playing an important role in bioprinting, printability (shear thinning) and shape fidelity (yield stress). [19]

At the inlet, an isotropic orientation of the fibers ($\psi = 1/\pi$) as a boundary condition was set. The results in Figure 5(A) show the ellipses initially circular and becoming gradually elongated along their

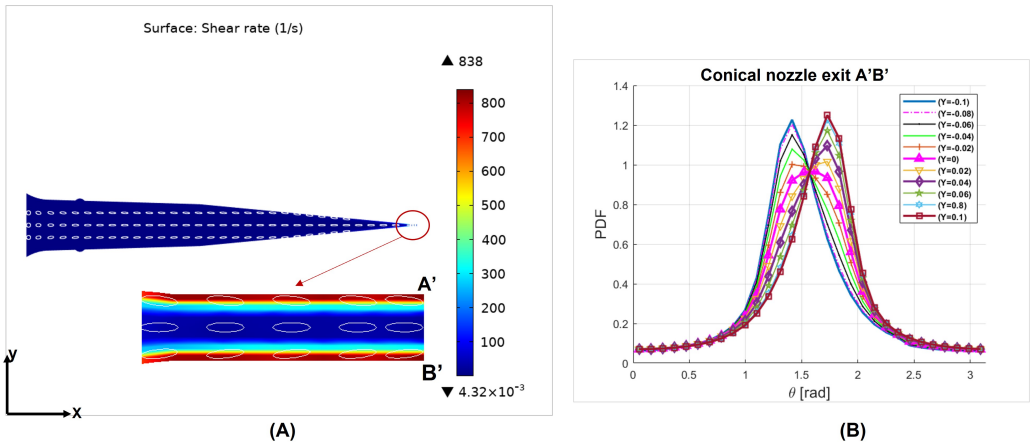

Figure 5: (A) Shear rate distribution and ellipses representing the average fiber orientation; (B) PDF's curves at outlet of the nozzle along the line A'B'.

major axes showing fibers alignment in the direction of the flow. The magnification of the outlet of the noozle in Figure 5(A) shows that along the x-axis at $y = 0$ (center-line of the nozzle), the fibers do not have a privileged orientation in contrast with the planar channel illustrated in Figure 4 and Figure 3 for both Newtonian and Herschel-Bulkley rheological behaviors. This result is depicted in Figure 5(B) by the pink triangle curve where the mean value of the orientation angle for the conical noozle is $\theta = 1.57 \pm 1.62$ rad compared to $\theta = 1.67 \pm 1.35$ rad for the panar channel. However, in the upper part between the wall and the center-line we notice a gradual orientation of the fibers leading to $\theta = 1.3$ rad at the upper part wall. Whereas, in the lower part the orientation angle reaches $\theta = 1.8$ rad at the upper part wall. This illustrates a symmetry of the orientation around the center-line of the nozzle driven by the shear rate.

4 Conclusion

In this work, a numerical strategy was implemented in to resolve the coupled problems of fiber motion and fluid flow in extrusion-based printing to predict the fiber orientation. It is based on a finite element discretization of the flow coupled to a hybrid finite element – finite volume discretization of the Fokker-Planck equation. The examples proposed have shown that the model can be used to compute the evolution and the final orientation of the rigid fibers in respect to the fluid rheological behavior and the geometry of the extrusion process. The model allows us to measure the alignment of any non-relaxing component along the axial direction of the extrusion. To validate the model several steps are planned. Experimental data will be acquired to compare the orientation of the fibers at the output of the nozzle in respect to the rheological behaviors. Also, the numerical simulation will be extended in 3D to consider the accuracy of the model. Finally, interaction between the fibers will be considered.

References

[1] N. Sigaux, L. Pourchet, P. Breton, S. Brosset, A. Louvrier, and C. Marquette, "3d bioprinting: principles, fantasies and prospects," *Journal of stomatology, oral and maxillofacial surgery*, vol. 120, no. 2, pp. 128–132, 2019.

[2] I. Doench, T. Ahn Tran, L. David, A. Montembault, E. Viguier, C. Gorzelanny, G. Sudre, T. Cachon, M. Louback-Mohamed, N. Horbelt *et al.*, "Cellulose nanofiber-reinforced chitosan hydrogel composites for intervertebral disc tissue repair," *Biomimetics*, vol. 4, no. 1, p. 19, 2019.

[3] A. Fatimi, O. V. Okoro, D. Podstawczyk, J. Siminska-Stanny, and A. Shavandi, "Natural hydrogel-based bio-inks for 3d bioprinting in tissue engineering: A review," *Gels*, vol. 8, no. 3, 2022. [Online]. Available: https://www.mdpi.com/2310-2861/8/3/179

[4] J. Y. Ng, S. Obuobi, M. L. Chua, C. Zhang, S. Hong, Y. Kumar, R. Gokhale, and P. L. R. Ee, "Biomimicry of microbial polysaccharide hydrogels for tissue engineering and regenerative medicine – a review," *Carbohydrate Polymers*, vol. 241, p. 116345, 2020. [Online]. Available: https://www.sciencedirect.com/science/article/pii/S0144861720305191

[5] A. Kamdem Tamo, I. Doench, L. Walter, A. Montembault, G. Sudre, L. David, A. Morales-Helguera, M. Selig, B. Rolauffs, A. Bernstein, D. Hoenders, A. Walther, and A. Osorio-Madrazo, "Development of bioinspired functional chitosan/cellulose nanofiber 3d hydrogel constructs by 3d printing for application in the engineering of mechanically demanding tissues," *Polymers*, vol. 13, no. 10, 2021. [Online]. Available: https://www.mdpi.com/2073-4360/13/10/1663

[6] A. Osorio-Madrazo, M. Eder, M. Rueggeberg, J. K. Pandey, M. J. Harrington, Y. Nishiyama, J.-L. Putaux, C. Rochas, and I. Burgert, "Reorientation of cellulose nanowhiskers in agarose hydrogels under tensile loading," *Biomacromolecules*, vol. 13, no. 3, pp. 850–856, 2012, pMID: 22295902. [Online]. Available: https://doi.org/10.1021/bm201764y

[7] H. Ravanbakhsh, G. Bao, and L. Mongeau, "Carbon nanotubes promote cell migration in hydrogels," *Scientific Reports*, vol. 10, no. 1, p. 2543, Feb. 2020. [Online]. Available: https://doi.org/10.1038/s41598-020-59463-9

[8] S. R. Shin, B. Aghaei-Ghareh-Bolagh, T. T. Dang, S. N. Topkaya, X. Gao, S. Y. Yang, S. M. Jung, J. H. Oh, M. R. Dokmeci, X. S. Tang, and A. Khademhosseini, "Cell-laden microengineered and mechanically tunable hybrid hydrogels of gelatin and graphene oxide," *Advanced Materials*, vol. 25, no. 44, pp. 6385–6391, 2013. [Online]. Available: https://onlinelibrary.wiley.com/doi/abs/10.1002/adma.201301082

[9] S. K. Kugler, A. Kech, C. Cruz, and T. Osswald, "Fiber orientation predictions—a review of existing models," *Journal of Composites Science*, vol. 4, no. 2, p. 69, 2020.

[10] S. G. Advani and C. L. Tucker III, "Closure approximations for three-dimensional structure tensors," *Journal of Rheology*, vol. 34, no. 3, pp. 367–386, 1990.

[11] G. B. Jeffery, "The motion of ellipsoidal particles immersed in a viscous fluid," *Proceedings of the Royal Society of London. Series A, Containing papers of a mathematical and physical character*, vol. 102, no. 715, pp. 161–179, 1922.

[12] F. Folgar and C. L. Tucker III, "Orientation behavior of fibers in concentrated suspensions," *Journal of reinforced plastics and composites*, vol. 3, no. 2, pp. 98–119, 1984.

[13] J. Férec, M. Heniche, M. Heuzey, G. Ausias, and P. Carreau, "Numerical solution of the fokker–planck equation for fiber suspensions: application to the folgar–tucker–lipscomb model," *Journal of non-newtonian fluid mechanics*, vol. 155, no. 1-2, pp. 20–29, 2008.

[14] D. Mezi, G. Ausias, S. G. Advani, and J. Férec, "Fiber suspension in 2d nonhomogeneous flow: The effects of flow/fiber coupling for newtonian and power-law suspending fluids," *Journal of Rheology*, vol. 63, no. 3, pp. 405–418, 2019.

[15] M. C. Altan, S. Subbiah, S. I. Güçeri, and R. B. Pipes, "Numerical prediction of three-dimensional fiber orientation in hele-shaw flows," *Polymer Engineering & Science*, vol. 30, no. 14, pp. 848–859, 1990.

[16] L. J. Pourchet, A. Thepot, M. Albouy, E. J. Courtial, A. Boher, L. J. Blum, and C. A. Marquette, "Human skin 3d bioprinting using scaffold-free approach," *Advanced Healthcare Materials*, vol. 6, no. 4, p. 1601101, 2017.

[17] L. Lemarié, A. Anandan, E. Petiot, C. Marquette, and E.-J. Courtial, "Rheology, simulation and data analysis toward bioprinting cell viability awareness," *Bioprinting*, vol. 21, p. e00119, 2021.

[18] I. T. Ozbolat, H. Chen, and Y. Yu, "Development of 'multi-arm bioprinter' for hybrid biofabrication of tissue engineering constructs," *Robotics and Computer-Integrated Manufacturing*, vol. 30, no. 3, pp. 295–304, 2014.

[19] A. Schwab, R. Levato, M. D'Este, S. Piluso, D. Eglin, and J. Malda, "Printability and shape fidelity of bioinks in 3d bioprinting," *Chemical reviews*, vol. 120, no. 19, pp. 11 028–11 055, 2020.